



**HAL**  
open science

## **ERG potassium channels and T-type calcium channels contribute to the pacemaker and atrioventricular conduction in zebrafish larvae**

Jussepe Salgado-Almario, Yillcer Molina, Manuel Vicente, Antonio Martínez-Sielva, Raúl Rodríguez-García, Pierre Vincent, Beatriz Domingo, Juan Llopis

### ► To cite this version:

Jussepe Salgado-Almario, Yillcer Molina, Manuel Vicente, Antonio Martínez-Sielva, Raúl Rodríguez-García, et al.. ERG potassium channels and T-type calcium channels contribute to the pacemaker and atrioventricular conduction in zebrafish larvae. *Acta Physiologica*, 2024, 240 (2), pp.e14075. 10.1111/apha.14075 . hal-04344031

**HAL Id: hal-04344031**

**<https://hal.science/hal-04344031v1>**

Submitted on 22 Nov 2024

**HAL** is a multi-disciplinary open access archive for the deposit and dissemination of scientific research documents, whether they are published or not. The documents may come from teaching and research institutions in France or abroad, or from public or private research centers.

L'archive ouverte pluridisciplinaire **HAL**, est destinée au dépôt et à la diffusion de documents scientifiques de niveau recherche, publiés ou non, émanant des établissements d'enseignement et de recherche français ou étrangers, des laboratoires publics ou privés.



Distributed under a Creative Commons Attribution - NonCommercial 4.0 International License

## RESEARCH PAPER

# ERG potassium channels and T-type calcium channels contribute to the pacemaker and atrioventricular conduction in zebrafish larvae

Jussepe Salgado-Almarino<sup>1</sup>  | Yillcer Molina<sup>1</sup>  | Manuel Vicente<sup>1</sup>  |  
 Antonio Martínez-Sielva<sup>1</sup>  | Raúl Rodríguez-García<sup>1</sup>  | Pierre Vincent<sup>2</sup>  |  
 Beatriz Domingo<sup>1</sup>  | Juan Llopis<sup>1</sup> 

<sup>1</sup>Physiology and Cell Dynamics,  
 Facultad de Medicina de Albacete,  
 Universidad de Castilla-La Mancha,  
 Albacete, Spain

<sup>2</sup>IGF, Univ. Montpellier, CNRS,  
 INSERM, Montpellier, France

## Correspondence

Juan Llopis and Beatriz Domingo,  
 Physiology and Cell Dynamics,  
 Facultad de Medicina de Albacete,  
 Universidad de Castilla-La Mancha, C/  
 Almansa 14, Albacete 02006, Spain.  
 Email: [juan.llopis@uclm.es](mailto:juan.llopis@uclm.es); [beatriz.domingo@uclm.es](mailto:beatriz.domingo@uclm.es)

## Funding information

Ministry of Science, Innovation and  
 Universities, Spain, Grant/Award  
 Number: PID2019-111456RB-100;  
 Consejería de Educación, Cultura y  
 Deportes, Junta de Comunidades de  
 Castilla-La Mancha, Grant/Award  
 Number: SBPLY/19/180501/000223;  
 EU FEDER-ERDF, Grant/Award  
 Number: 2021-GRIN-31151,  
 2020-GRIN-29186, 2019-GRIN-27019  
 and SBPLY/19/180501/000223;  
 University of Castilla-La  
 Mancha, Grant/Award Number:  
 2021-GRIN-31151, 2020-GRIN-29186  
 and 2019-GRIN-27019

## Abstract

**Aim:** Bradyarrhythmias result from inhibition of automaticity, prolonged repolarization, or slow conduction in the heart. The ERG channels mediate the repolarizing current  $I_{Kr}$  in the cardiac action potential, whereas T-type calcium channels (TTCC) are involved in the sinoatrial pacemaker and atrioventricular conduction in mammals. Zebrafish have become a valuable research model for human cardiac electrophysiology and disease. Here, we investigate the contribution of ERG channels and TTCCs to the pacemaker and atrioventricular conduction in zebrafish larvae and determine the mechanisms causing atrioventricular block.

**Methods:** Zebrafish larvae expressing ratiometric fluorescent  $Ca^{2+}$  biosensors in the heart were used to measure  $Ca^{2+}$  levels and rhythm in beating hearts in vivo, concurrently with contraction and hemodynamics. The atrioventricular delay (the time between the start of atrial and ventricular  $Ca^{2+}$  transients) was used to measure impulse conduction velocity and distinguished between slow conduction and prolonged refractoriness as the cause of the conduction block.

**Results:** ERG blockers caused bradycardia and atrioventricular block by prolonging the refractory period in the atrioventricular canal and in working ventricular myocytes. In contrast, inhibition of TTCCs caused bradycardia and second-degree block (Mobitz type I) by slowing atrioventricular conduction. TTCC block did not affect ventricular contractility, despite being highly expressed in cardiomyocytes. Concomitant measurement of  $Ca^{2+}$  levels and ventricular size showed mechano-mechanical coupling: increased preload resulted in a stronger heart contraction in vivo.

**Conclusion:** ERG channels and TTCCs influence the heart rate and atrioventricular conduction in zebrafish larvae. The zebrafish lines expressing  $Ca^{2+}$

Yillcer Molina and Manuel Vicente contributed equally.

This is an open access article under the terms of the [Creative Commons Attribution-NonCommercial](https://creativecommons.org/licenses/by-nc/4.0/) License, which permits use, distribution and reproduction in any medium, provided the original work is properly cited and is not used for commercial purposes.

© 2023 The Authors. *Acta Physiologica* published by John Wiley & Sons Ltd on behalf of Scandinavian Physiological Society.

biosensors in the heart allow us to investigate physiological feedback mechanisms and complex arrhythmias.

#### KEYWORDS

atrioventricular block, calcium, ERG potassium channel, heart, T-type calcium channel, zebrafish

## 1 | INTRODUCTION

In humans, malfunction of the pacemaker, the sinoatrial node (SAN), gives rise to inappropriate heart rate (HR), whereas alterations of atrioventricular (AV) conduction result in various types of AV block, resulting in bradyarrhythmia. In recent years, zebrafish has become an attractive vertebrate model to study heart development, regeneration, and heart disease,<sup>1–3</sup> and as much as 71% of human genes have one or more orthologs in zebrafish.

The zebrafish heart is composed of only two chambers, atrium and ventricle, but its electrophysiology in larvae and adults has many similarities with the human heart.<sup>4–8</sup> The electrical excitation in zebrafish starts at the sinoatrial (SA) ring, a ring-like structure with pacemaker activity, spreads through the atrium and reaches the AV canal, which delays electrical conduction to allow the ventricle to fill with blood prior to contraction. As in humans, the ventricular action potential (AP) in zebrafish has a plateau phase (phase 2) due to  $\text{Ca}^{2+}$  influx through L-type voltage-dependent  $\text{Ca}^{2+}$  channels (LTCCs). In addition, the HR (110–130 beats per minute in adult fish), the AP duration (APD), and the ECG, including the QT interval, are also alike.<sup>9,10</sup> However, differences in ion channel composition and in excitation–contraction coupling have also been found.<sup>5,11,12</sup> Thus, T-type  $\text{Ca}^{2+}$  channels (TTCCs) are much more abundant in the zebrafish heart than in the adult mammalian heart and may contribute to excitation–contraction coupling.

The “rapid” delayed rectifier potassium current ( $I_{\text{Kr}}$ ) is the main repolarizing current in the human heart. The channel underlying  $I_{\text{Kr}}$  ( $\text{K}_{\text{v}}11.1$ ) is encoded by the human ether-a-go-go-related gene (*hERG* or *KCNH2*). Mutations in this gene or drugs that block hERG prolong the APD and cause long QT syndrome. In the zebrafish heart,  $I_{\text{Kr}}$  is determined predominantly by *kcnh6a* (*zerg* or  $\text{K}_{\text{v}}11.2$ ).<sup>5–7,13</sup> Although the current is produced by a different ERG isoform, the zebrafish heart is sensitive to  $I_{\text{Kr}}$  blockers which prolong the QT interval because the channel pore and drug-binding regions are nearly identical.<sup>14,15</sup> The zebrafish mutant *breakdance*, which holds a mutation in *kcnh6a*, is characterized by a 2:1 AV block due to prolonged refractoriness.<sup>15,16</sup>

Mechanisms other than APD prolongation such as slow conduction velocity may lead to AV blocks. In mammals,  $\text{Ca}_{\text{v}}3.1$  (T-type) and  $\text{Ca}_{\text{v}}1.3$  channels are involved in automaticity of the SAN and conduction in the AV node,<sup>17–20</sup> and alterations of these channels have been associated with congenital bradycardia and heart block disease in humans.<sup>21,22</sup> In zebrafish larvae,  $\text{Ca}_{\text{v}}3.1$  (*cacna1g*) transcripts encoding TTCCs are enriched in the SA ring and AV canal,<sup>23,24</sup> although their functional relevance is yet unknown. TTCCs are also highly expressed in zebrafish atrial and ventricular myocytes,<sup>5,8,25</sup> in contrast with the adult human heart, in which LTCCs ( $\text{Ca}_{\text{v}}1.2$   $\alpha$ -subunit) represent 96%–98% of the transcripts,<sup>8</sup> although  $\text{Ca}_{\text{v}}3.1$  channel protein has recently been detected in working cardiomyocytes from mice.<sup>26</sup>

As in mammals,  $\text{Ca}^{2+}$  is central in excitation–contraction coupling and largely determines force generation.<sup>27</sup> We have recently imaged  $\text{Ca}^{2+}$  and contraction simultaneously in beating hearts of zebrafish expressing ratio-metric gene-encoded  $\text{Ca}^{2+}$  biosensors,<sup>28,29</sup> preserving the mechano-electric and mechano-mechanical coupling<sup>30</sup> and normal heart development. In the present study, we show the involvement of TTCCs in the conduction system of zebrafish larvae and characterize AV conduction defects induced by block of TTCCs and ERG channels. We measured the delay between atrial and ventricular  $\text{Ca}^{2+}$  transients to estimate the conduction velocity to distinguish the mechanism of the AV block and determine its functional repercussion.

## 2 | RESULTS

### 2.1 | Changes in heart rhythm, $\text{Ca}^{2+}$ levels, and contraction induced by blocking ERG channel with dofetilide

In mammals, the class III anti-arrhythmic drug dofetilide prolongs the APD, blocking the rapid component of the delayed rectifier  $\text{K}^{+}$  current  $I_{\text{Kr}}$ <sup>31</sup> with no effect on the other repolarizing currents ( $I_{\text{Ks}}$ ,  $I_{\text{K1}}$ ). In zebrafish cardiomyocytes, dofetilide was shown to prolong the APD<sub>50</sub> by 70 ms.<sup>3</sup> We tested the effects of dofetilide on the heart rhythm,  $\text{Ca}^{2+}$  levels, and contractility in

3- and 5-days post-fertilization (dpf) zebrafish larvae expressing the ratiometric  $\text{Ca}^{2+}$  biosensor Twitch-4 in the heart. Although the  $K_i$  of dofetilide for hERG ( $K_{v11.1}$ ) channels is 6.4 nM, larvae incubated with 1 or 10  $\mu\text{M}$  dofetilide for up to 2 h did not show a significant change in HR or rhythm (Table S1). Incubation of 3 dpf *Tg(myl7:Twitch-4)* larvae with 100  $\mu\text{M}$  dofetilide caused bradycardia and, after 1.5 h, a 2:1 arrhythmia (one ventricular contraction every two atrial beats) (Figure 1A,B, Table 1, Movie S1 and S2). This drug concentration is much higher than that used in cell systems since the embryonic skin and the agarose layer pose a diffusion barrier to drugs.<sup>15</sup>  $\text{Ca}^{2+}$  levels decreased in the ventricle and increased in the atrium after the appearance of the 2:1 arrhythmia (Figure 1B) and the ventricular and atrial  $\text{Ca}^{2+}$  transient (CaT) amplitude increased. There was no effect of the solvent DMSO (1%), except for the HR, which increased slightly with time (Table S2). At 5 dpf, all larvae displayed 2:1 arrhythmia after addition of dofetilide (100  $\mu\text{M}$ , 1 h) (Figure S1A–D, Movie S3 and S4), and 4 out of 9 larvae showed ventricular arrest after 2 h, suggesting a complete block of AV conduction or ventricular inexcitability (Figure S1E).

Interestingly, the time between the start of atrial and ventricular CaTs (hereafter referred to as the AV delay) decreased from  $77 \pm 7$  to  $52 \pm 9$  ms ( $n=9$ ,  $p < 0.0001$ ) in 3 dpf larvae with 2:1 arrhythmia (Figure 1C, Table 1). It also decreased at 5 dpf (Figure S1C). This delay informs about AV conduction velocity, and we propose that it is analogous to the PR interval of the ECG but reports the delay between atrial and ventricular CaT rather than electrical activation. Thus, AV conduction velocity increased during 2:1 arrhythmia induced by dofetilide. It can be classed as a second-degree AV block type 2:1 since the AV delay was regular.

The effects of dofetilide were reversible. After 17–24 min incubation with 100  $\mu\text{M}$  dofetilide (3 dpf larvae not embedded in agarose), atrial bradycardia (85% of basal HR) was observed, and 2:1 block was visible in 93% of larvae (Figure S2A). Note that the effect of the drug was fivefold faster in E3 medium than in larvae embedded in agarose (Figure 1). After 60 min washout of the drug, 71% of larvae recovered the normal 1:1 atrial to ventricular beat ratio, and the atrial HR was 95% of the basal rate. After 80 min washout, all larvae had normal ventricular contraction and HR (Figure S2A).

We further investigated the effect of dofetilide on AV conduction in 3 dpf larvae pretreated with the myosin inhibitor *para*-aminoblebbistatin to stop the heart (Figure 1E), which allowed us to measure  $\text{Ca}^{2+}$  in small areas of the heart. In larvae showing a 2:1 arrhythmia, dofetilide caused a widening of the CaT at the level of the AV canal and in the ventricle, likely caused by

prolongation of the APD in these areas (Movie S5 and S6).

In humans, second-degree AV blocks pose a clinical problem when inadequate ventricular rate fails to meet the physiological needs. We estimated the contractility and hemodynamic outcome of the 2:1 block induced by dofetilide. Since there were two atrial beats for each ventricular beat, the fractional area change (FAC) and stroke volume (SV) increased by 22% and 31%, respectively (Figure 1D). However, due to the low HR, the cardiac output (CO) decreased. Similar results were found at 5 dpf (Figure S1D). Therefore, blocking zerg channels with dofetilide impaired automatism and AV conduction in zebrafish larvae, causing bradycardia, a second-degree AV block, and ventricular arrest. In humans, bradycardia, AV block, or bundle branch block are common adverse effects of dofetilide.

## 2.2 | Prolongation of the refractory period by dofetilide and altered ventricular filling

To further study the consequences of the 2:1 arrhythmia on ventricular filling, we correlated the changes in ventricular diameter with  $\text{Ca}^{2+}$  levels in real time (Figure 2). Six out of nine larvae displaying 2:1 arrhythmia showed biphasic ventricular filling: both the blocked and the conducted atrial beats filled the ventricle (Figure 2A, blue line). In the remaining larvae (Figure 2B), the blocked atrial beat did not cause much ventricular filling as the ventricle remained contracted (orange-dashed line), but the following atrial beat did (red-dashed line). The diameter versus ventricular  $\text{Ca}^{2+}$  plots shows two fillings (Figure 2A, right panel) or one predominant filling (Figure 2B, right panel) for each ventricular systole. The ventricular  $\text{Ca}^{2+}$  plateau (measured as the time between the 90% rise and 10% decay of the CaT) was longer in larvae with no filling during the AV block than in those displaying biphasic ventricular filling (Figure 2B vs 2A) ( $150 \pm 16$  vs  $119 \pm 11$  ms, respectively,  $p = 0.026$ ), which explains the prolonged ventricular contraction in the former group.

Figure 2C shows a 2:1 AV block which began in the course of image acquisition: during the first dropped ventricular beat, there was partial filling of the ventricle by atrial contraction (orange-dashed line). In successive beats, the ventricular CaT showed a plateau and, progressively, the ventricle remained more contracted (blue arrows). This result suggests a gradual prolongation of the ventricular APD and refractory period by the  $I_{Kr}$  blocker in the ventricular myocardium. Unlike the observations at 3 dpf, in all 5 dpf larvae the blocked atrial beat (orange-dashed line) almost filled the ventricle (increased

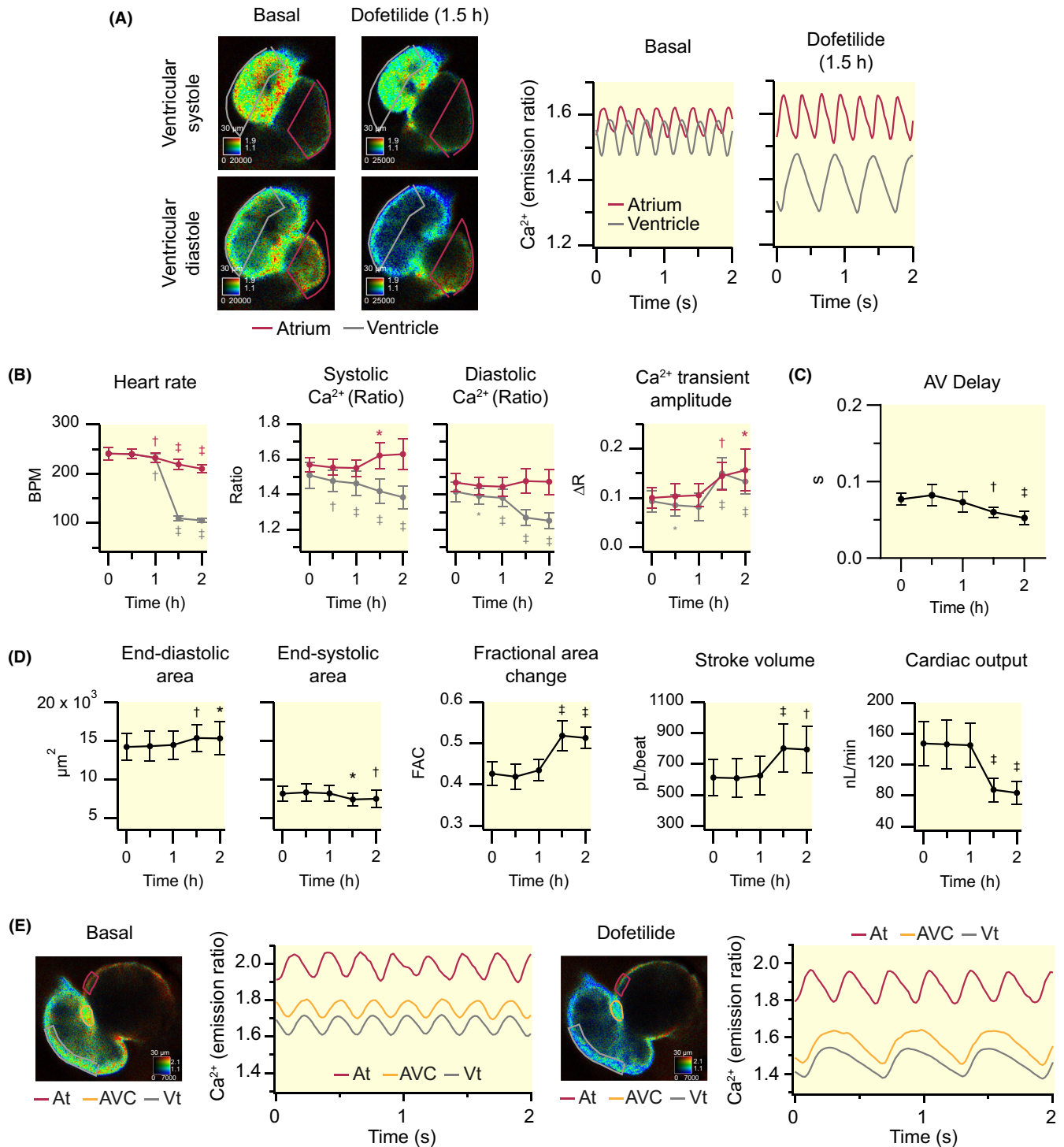


**FIGURE 1** Effect of dofetilide on cardiac Ca<sup>2+</sup> levels and ventricular contractility of 3 dpf zebrafish larvae. Dofetilide (100 μM) was added to *Tg(myl7:Twitch-4)* larvae at 3 dpf ( $N=3$ ,  $n=9$ ) after recording basal Ca<sup>2+</sup> levels. (A) Emission ratio images of a representative larva before (basal) and after 1.5 h incubation with dofetilide. The calibration squares show the distance in μm (top side), the emission ratio coded in the hue (right side), and the fluorescence intensity (bottom side). The traces show the atrial (red) and ventricular (gray) Ca<sup>2+</sup> levels (emission ratio). (B) Effect of dofetilide on heart rate, systolic and diastolic Ca<sup>2+</sup> levels, and Ca<sup>2+</sup> transient amplitude in the atrium (red) and ventricle (gray). (C) Effect of dofetilide on the AV delay (time between the start of atrial and ventricular Ca<sup>2+</sup> transients). (D) Effect of dofetilide on ventricular areas, fractional area change, stroke volume, and cardiac output. (E) Effect of dofetilide on AV conduction in a 3 dpf zebrafish larva whose heart was stopped by incubation with the myosin inhibitor *para*-aminoblebbistatin (75 μM for 2 h) (representative experiment). ROIs were drawn as indicated to investigate the progression of the Ca<sup>2+</sup> wave from the atrium (At), across the AV canal (AVC), and into the ventricle (Vt). The traces show the time course of the Ca<sup>2+</sup> transients in each ROI. Data in B, C, and D are shown as the mean ± SD. Statistical analysis was performed using a one-way ANOVA test with Dunnett's multiple comparisons post-test (\* $p < 0.05$ , † $p < 0.01$ , ‡ $p < 0.001$ ).

TABLE 1 Effect of dofetilide on HR, cardiac Ca<sup>2+</sup> levels, and ventricular contractility of 3 dpf zebrafish larvae.

Parameter	Cardiac chamber	n	Time points				
			Basal	0.5h	1h	1.5h	2h
Heart rate (bpm)	Atrium	9	240.7 ± 12.6	239.9 ± 9.6 <sup>†</sup>	232.4 ± 9.2 <sup>‡</sup>	218.8 ± 9.9 <sup>‡</sup>	210.0 ± 8.6 <sup>‡</sup>
	Ventricle	9	240.7 ± 12.7	239.9 ± 9.5 <sup>†</sup>	232.1 ± 9.0 <sup>‡</sup>	109.4 ± 5.0 <sup>‡</sup>	105.3 ± 4.3 <sup>‡</sup>
Systolic Ca <sup>2+</sup> (ratio)	Atrium	9	1.57 ± 0.04	1.55 ± 0.05	1.55 ± 0.05	1.62 ± 0.07*	1.63 ± 0.09
	Ventricle	9	1.51 ± 0.07	1.48 ± 0.06 <sup>†</sup>	1.46 ± 0.07 <sup>‡</sup>	1.42 ± 0.07 <sup>‡</sup>	1.38 ± 0.06 <sup>‡</sup>
Diastolic Ca <sup>2+</sup> (ratio)	Atrium	9	1.47 ± 0.05	1.45 ± 0.05	1.44 ± 0.05	1.48 ± 0.07	1.47 ± 0.07
	Ventricle	9	1.42 ± 0.06	1.39 ± 0.05*	1.38 ± 0.05 <sup>‡</sup>	1.27 ± 0.05 <sup>‡</sup>	1.25 ± 0.04 <sup>‡</sup>
CaT amplitude (ratio)	Atrium	9	0.10 ± 0.02	0.10 ± 0.03	0.11 ± 0.02	0.14 ± 0.03 <sup>†</sup>	0.15 ± 0.04*
	Ventricle	9	0.09 ± 0.02	0.085 ± 0.02*	0.08 ± 0.02	0.15 ± 0.02 <sup>‡</sup>	0.13 ± 0.02 <sup>‡</sup>
AV delay (s)	–	9	0.077 ± 0.008	0.082 ± 0.014	0.073 ± 0.013	0.060 ± 0.007 <sup>†</sup>	0.053 ± 0.009 <sup>‡</sup>
End-diastolic area (μm <sup>2</sup> )	Ventricle	9	14 200 ± 1751	14 308 ± 1958	14 464 ± 1838	15 357 ± 1751 <sup>†</sup>	15 315 ± 2158*
End-systolic area (μm <sup>2</sup> )	Ventricle	9	8134 ± 1003	8293 ± 1091	8163 ± 990	7369 ± 814*	7454 ± 1112 <sup>†</sup>
Fractional area change	Ventricle	9	0.43 ± 0.03	0.42 ± 0.03	0.44 ± 0.03	0.52 ± 0.04 <sup>‡</sup>	0.51 ± 0.03 <sup>‡</sup>
Stroke volume (pL/beat)	Ventricle	9	612.8 ± 119.5	608.6 ± 125.0	626.0 ± 125.4	802.2 ± 155.7 <sup>‡</sup>	794.4 ± 149.2 <sup>†</sup>
Cardiac output (nL/min)	Ventricle	9	147.5 ± 28.3	146.4 ± 31.4	145.3 ± 28.9	87.5 ± 15.4 <sup>‡</sup>	83.5 ± 14.9 <sup>‡</sup>

Note: Data are shown as the mean ± SD. Statistical analysis was done as indicated in Figure 1. *Tg(myl7:Twitch-4)* larvae were treated with 100 μM dofetilide for 2h with imaging recording every 30 min.

\**p* < 0.05.

<sup>†</sup>*p* < 0.01.

<sup>‡</sup>*p* < 0.001.

diameter) (Figure 2D), suggesting that the ventricle was out of its refractory period and the block was at the AV canal.

### 2.3 | Changes of Ca<sup>2+</sup> levels and contraction during arrhythmia induced by drugs with ERG channel blocking activity as an adverse effect

We also examined the arrhythmogenic effects of three other drugs known to block I<sub>Kr</sub>, the antihistamines terfenadine and astemizole, which were withdrawn from the market because of causing severe arrhythmic events, and the psychotropic drug haloperidol. Terfenadine is a potent hERG blocker, which induces prolongation of the QT interval of the ECG and AV block.<sup>32</sup> It has been shown to cause bradycardia and arrhythmia in zebrafish.<sup>15</sup> Alday et al<sup>4</sup> found that terfenadine prolonged the APD<sub>90</sub> in 2 dpf zebrafish embryos, indicating the role of I<sub>Kr</sub> in phase 3 of the AP. In addition, in paced embryonic ventricles, terfenadine prolonged the APD such that only every other stimulus was able to elicit an AP (2:1 block).<sup>33</sup> It has been reported that the treatment of 3 dpf zebrafish larvae with 10 μM terfenadine for 24h reproduced some features of heart failure.<sup>34,35</sup> We investigated the effects of terfenadine (20 μM for 24h) on heart rhythm, Ca<sup>2+</sup> levels, and contractility in 3 dpf

larvae. One group of larvae (10 out of 28) showed bradycardia and decreased ventricular Ca<sup>2+</sup> levels at 4 dpf (Figure S3A,B, Movie S7 and S8). In the remaining larvae, in addition to atrial bradycardia, a 2:1 arrhythmia appeared, with a marked increase of the ventricular CaT amplitude with reduced diastolic Ca<sup>2+</sup> (Figure S3A,B, Movie S9), in keeping with the low ventricular HR.<sup>12</sup>

Concerning the effect of terfenadine on ventricular contraction, in larvae showing bradycardia the end-diastolic and end-systolic areas increased, but CaT amplitude and the FAC were not affected (Figure S3B,C). Likewise, the SV and CO did not change. In contrast, larvae showing 2:1 arrhythmia, with a low ventricular HR of about 84 ± 8 bpm (*n* = 18) and increased CaT amplitude (Figure S3B), displayed enhanced FAC and SV (Figure S3C), but the CO decreased. Similar effects of terfenadine regarding HR, AV decoupling, and blood flow have been reported in 4 dpf zebrafish.<sup>1,36</sup>

To test the I<sub>Kr</sub> blockers astemizole and haloperidol and to rule out indicator-dependent effects, we used two other transgenic zebrafish lines raised in our laboratory with the cardiac Ca<sup>2+</sup> biosensors Twitch-1 (higher Ca<sup>2+</sup> affinity than Twitch-4)<sup>37</sup> and mCyRFP1-GCaMP6f (with calmodulin as the Ca<sup>2+</sup> binding domain),<sup>29</sup> respectively. Incubation of *Tg(myl7:Twitch-1)* larvae with astemizole for 45 min (50 μM) caused atrial bradycardia and 2:1 arrhythmia. It also decreased Ca<sup>2+</sup> levels and increased CaT amplitude in the ventricle (Table S3). In contrast, the FAC and SV

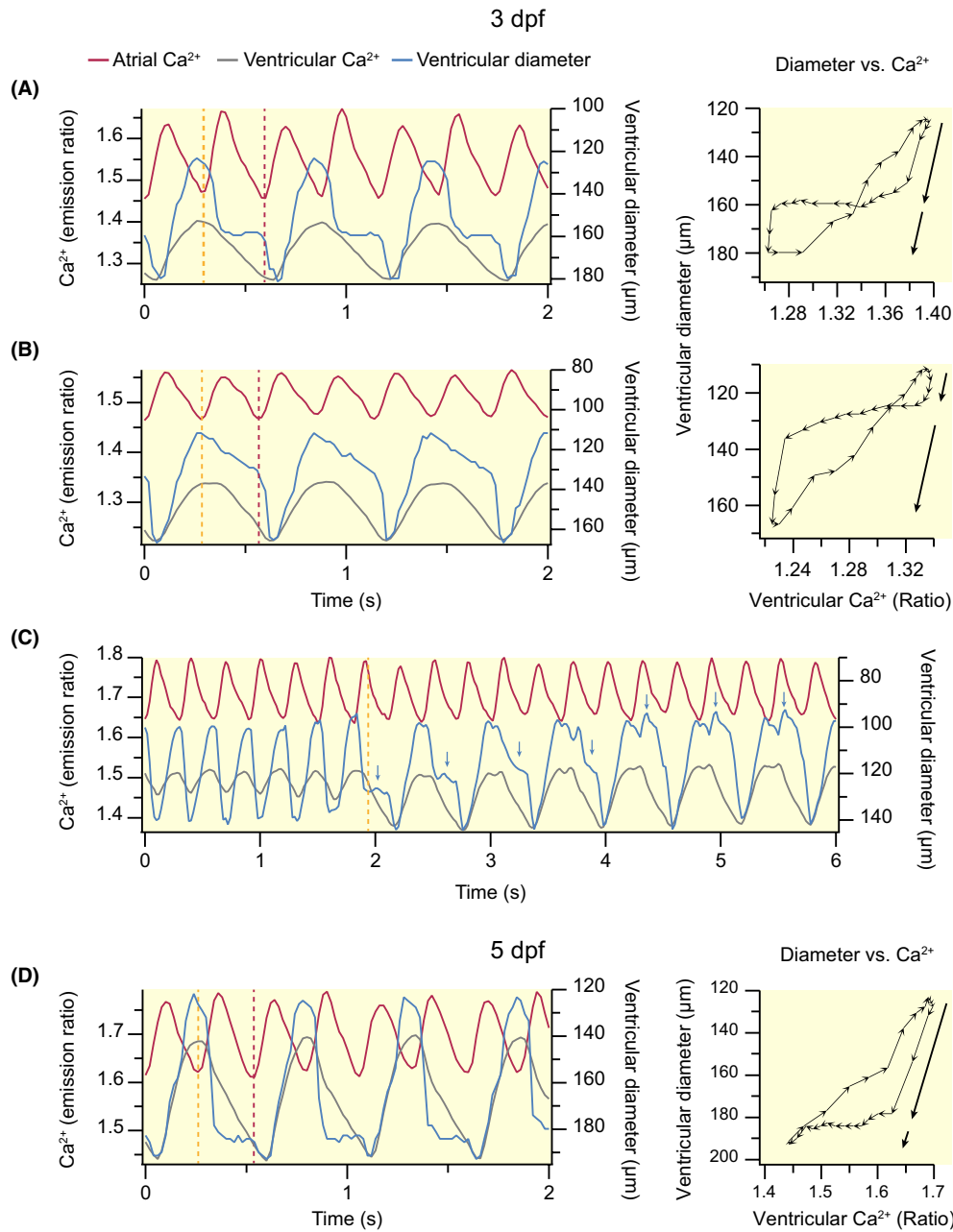


**FIGURE 2** Alterations in ventricular filling during dofetilide-induced AV block in 3 (A–C) and 5 (D) dpf *Tg(myl7:Twitch-4)* zebrafish larvae. The traces show the atrial (red) and ventricular (gray) Ca<sup>2+</sup> levels, and the major ventricular diameter (blue). The dashed lines indicate the start of the atrial CaT that was not conducted to the ventricle (orange), and the start of the next, conducted, atrial CaT (red). In some larvae (A), both blocked and conducted atrial contractions filled the ventricle with blood, whereas in others the first (B) or the second (D) atrial contraction hardly modified the ventricular diameter. Blue arrows in C indicate the level of ventricular filling at the end of the first atrial beat. The diagrams (diameter vs. Ca<sup>2+</sup>) show the ventricular diameter versus ventricular Ca<sup>2+</sup> level (one cardiac cycle) of representative larvae. The distance between arrowheads in these loops represents 20 ms, showing the direction of time and the relative speed of each phase. The black arrows show the two-step increase in ventricular diameter during ventricular filling.

did not change, but the bradycardia caused a decline in CO. Finally, haloperidol in 3 dpf *Tg(myl7:mCyRFP1-GCaMP6f)* larvae showed effects like the other I<sub>Kr</sub> blockers. Incubation of larvae with 100 µM haloperidol for 45 min caused atrial bradycardia and, in 57% of treated larvae, a 2:1 arrhythmia (Table S3). Ventricular CaT amplitude

increased, the FAC and SV rose, whereas the AV delay and CO were reduced.

In conclusion, blocking of ERG channels with various drugs decreased automaticity and caused second-degree AV block by prolonging the APD at the level of the AV canal and, in some larvae, in the ventricle.

## 2.4 | The T-type $\text{Ca}^{2+}$ channel blocker ML218 induced bradycardia and second-degree AV block in zebrafish larvae by slowing AV conduction

TTCCs are involved in the SAN pacemaker and AV conduction in mammals and are also expressed in working cardiomyocytes in newborn mice and in diseased human

heart.<sup>8,17,22</sup> We studied the functional role of TTCCs in zebrafish heart. We incubated 3 dpf *Tg(myf7:Twitch-4)* larvae with the TTCC antagonist ML218 at 0.01, 0.1, 0.3, and 1 mM to test its effects on automaticity, AV conduction, and  $\text{Ca}^{2+}$  levels in atrium and ventricle. No effects were observed at 0.01 and 0.1 mM ML218 (Table S4). Incubation of larvae with 0.3 mM ML218 for 1 h induced bradycardia (Figure 3A, Table 2, Movie S10 and S11) and

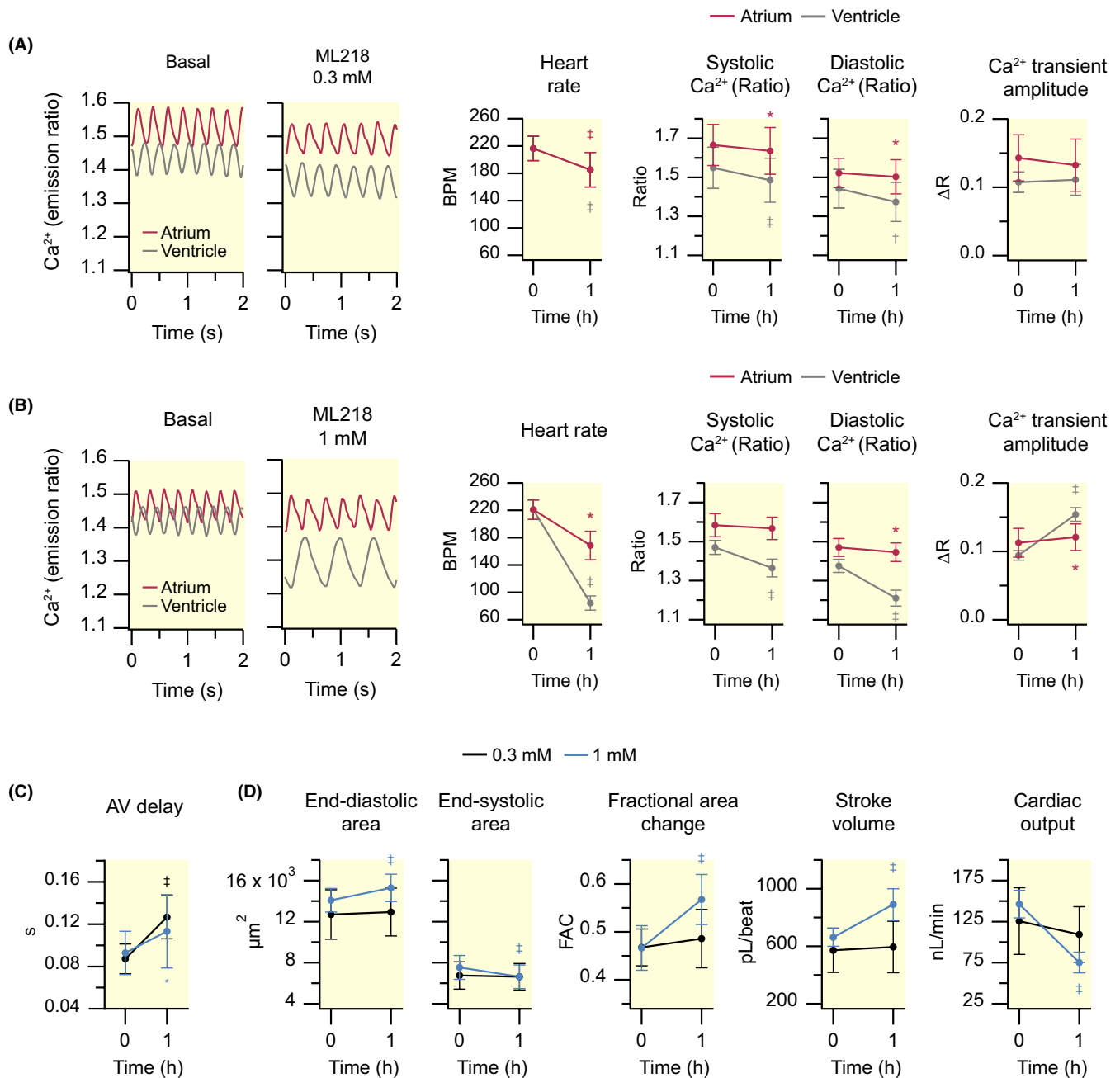


**FIGURE 3** Effect of the T-type  $\text{Ca}^{2+}$  channel antagonist ML218 (0.3 and 1 mM) on cardiac  $\text{Ca}^{2+}$  levels and ventricular contractility of 3 dpf zebrafish larvae. *Tg(myf7:Twitch-4)* larvae at 3 dpf were treated with 0.3 mM ( $N=3$ ,  $n=11$ ) or 1 mM ( $N=3$ ,  $n=12$ ) ML218 for 1 h. Heart rate, systolic and diastolic  $\text{Ca}^{2+}$  levels, and  $\text{Ca}^{2+}$  transient amplitude in the atrium (red) and ventricle (gray) of larvae treated with 0.3 (A) or 1 mM (B) ML218. The traces in A and B show the atrial (red) and ventricular (gray)  $\text{Ca}^{2+}$  levels (emission ratio). AV delay (C), ventricular areas, fractional area change, stroke volume, and cardiac output (D) of larvae treated with 0.3 (black) or 1 mM (blue) ML218. Data are shown as the mean  $\pm$  SD. Statistical analysis in A and B was performed using a paired Student's *t* test, as well as in C and D for 0.3 mM ML218. Differences in C and D for 1 mM ML218 were analyzed using a Wilcoxon test (\* $p < 0.05$ , † $p < 0.01$ , ‡ $p < 0.001$ ).



**TABLE 2** Effect of the T-type  $\text{Ca}^{2+}$  channel antagonist ML218 (0.3 and 1 mM) on HR, cardiac  $\text{Ca}^{2+}$  levels, and ventricular contractility of 3 dpf zebrafish larvae.

Parameter	ML218 concentration (mM)	n	Cardiac chamber	Basal	After treatment
Heart rate (bpm)	0.3	11	Atrium	216.5 ± 17.8	185.2 ± 17.8 <sup>‡</sup>
			Ventricle	216.5 ± 17.9	185.3 ± 25.3 <sup>‡</sup>
	1	12	Atrium	220.9 ± 14.1	168.7 ± 20.9*
			Ventricle	220.8 ± 14.2	84.4 ± 10.5 <sup>‡</sup>
Systolic $\text{Ca}^{2+}$ (ratio)	0.3	11	Atrium	1.67 ± 0.10	1.64 ± 0.12*
			Ventricle	1.55 ± 0.11	1.49 ± 0.11 <sup>‡</sup>
	1	12	Atrium	1.58 ± 0.06	1.57 ± 0.06
			Ventricle	1.47 ± 0.04	1.36 ± 0.05 <sup>‡</sup>
Diastolic $\text{Ca}^{2+}$ (ratio)	0.3	11	Atrium	1.52 ± 0.07	1.50 ± 0.09*
			Ventricle	1.44 ± 0.10	1.37 ± 0.10 <sup>†</sup>
	1	12	Atrium	1.47 ± 0.05	1.45 ± 0.05*
			Ventricle	1.38 ± 0.03	1.21 ± 0.04 <sup>‡</sup>
CaT amplitude (ratio)	0.3	11	Atrium	0.143 ± 0.034	0.133 ± 0.037
			Ventricle	0.109 ± 0.016	0.112 ± 0.023
	1	12	Atrium	0.113 ± 0.021	0.122 ± 0.018*
			Ventricle	0.094 ± 0.008	0.153 ± 0.011 <sup>‡</sup>
AV delay (s)	0.3	11	–	0.087 ± 0.014	0.127 ± 0.020 <sup>‡</sup>
	1	12	–	0.093 ± 0.020	0.113 ± 0.035*
End-diastolic area ( $\mu\text{m}^2$ )	0.3	11	Ventricle	12700 ± 2407	12938 ± 2319
	1	12	Ventricle	14083 ± 1151	15288 ± 1330 <sup>‡</sup>
End-systolic area ( $\mu\text{m}^2$ )	0.3	11	Ventricle	6753 ± 1330	6635 ± 1286
	1	12	Ventricle	7544 ± 1161	6631 ± 1149 <sup>‡</sup>
Fractional area change	0.3	11	Ventricle	0.47 ± 0.04	0.49 ± 0.06
	1	12	Ventricle	0.47 ± 0.05	0.58 ± 0.05 <sup>‡</sup>
Stroke volume (pL/beat)	0.3	11	Ventricle	572.1 ± 154.1	595.3 ± 179.5
	1	12	Ventricle	662.4 ± 62.3	891.1 ± 109.3 <sup>‡</sup>
Cardiac output (nL/min)	0.3	11	Ventricle	125.6 ± 40.6	109.3 ± 33.7
	1	12	Ventricle	146.2 ± 16.8	75.2 ± 12.6 <sup>‡</sup>

Note: Data are shown as the mean ± SD. Statistical analysis was done as indicated in Figure 3. *Tg(myl7:Twitch-4)* larvae at 3 dpf were treated with 0.3 or 1 mM ML218 for 1 h.

\* $p < 0.05$ .

<sup>†</sup> $p < 0.01$ .

<sup>‡</sup> $p < 0.001$ .

decreased systolic and diastolic  $\text{Ca}^{2+}$  levels, but CaT amplitude did not change. These larvae with low HR displayed slow AV conduction, since the AV delay increased from  $87 \pm 14$  to  $127 \pm 20$  ms ( $n = 11$ ,  $p < 0.0001$ ) (Figure 3C, Table 2). There was no significant change in the FAC, SV, and CO (Figure 3D).

The rise time of the CaT in the ventricle increased by incubation with 0.3 mM ML218 for 1 h ( $81 \pm 8$  vs  $95 \pm 16$  ms,  $p = 0.002$ , before vs after ML218); the atrial rise time was not significantly different ( $56 \pm 5$  vs  $59 \pm 5$  ms,  $p = 0.092$ , before vs after ML218). This suggests that TTCCs, with a low-voltage threshold for activation of about  $-70$  mV,

contribute to a fast-rising CaT earlier than the LTCCs ( $-40$  mV threshold).

Interestingly, in 7 out of 30 larvae with marked bradycardia, a ventricular CaT and beat were missing every three, four, or more atrial CaT (Figure 4A,B, Movie S12). In these larvae, there was a progressive prolongation of the AV delay from 150 to 300 ms (Figure 4C); at that point one atrial impulse was not conducted to the ventricle. This is reminiscent of a second-degree AV block of the Mobitz type I (Wenckebach) in humans, in which there is a progressive PR interval prolongation before a “dropped beat” occurs. In larvae with dropped beats, the first AV delay after the block

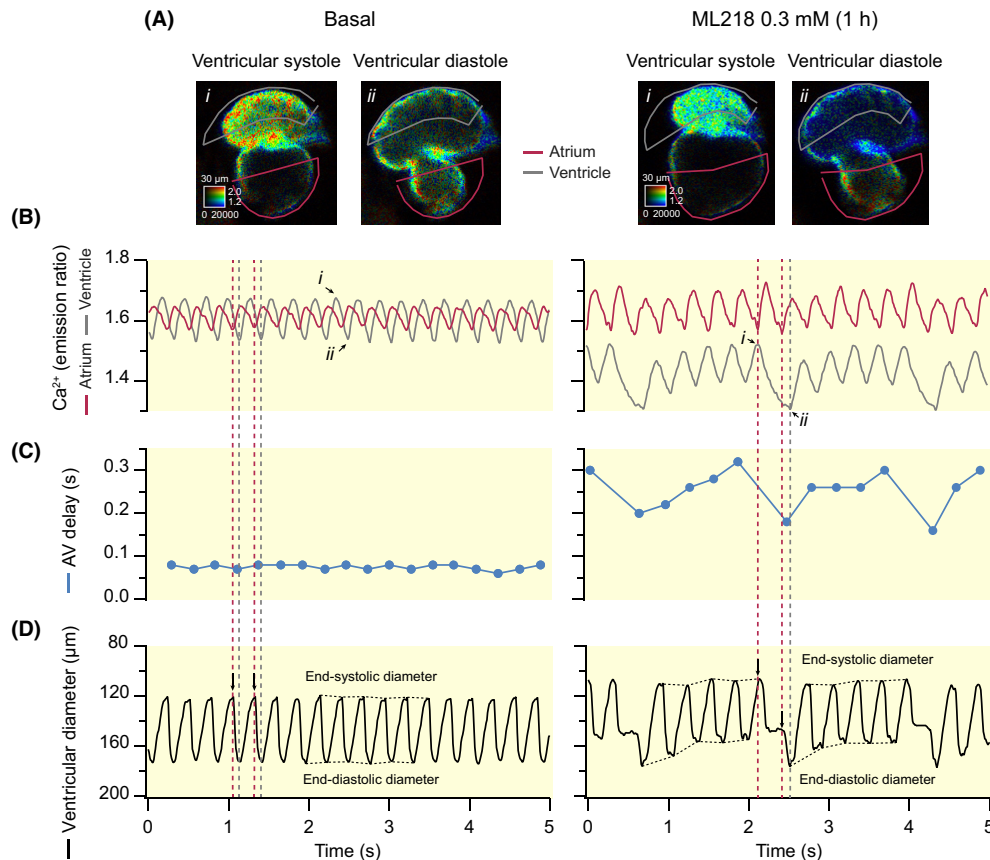


**FIGURE 4** Second-degree AV block of Mobitz type I in a representative 3 dpf zebrafish larva induced by the T-type  $\text{Ca}^{2+}$  channel antagonist ML218 (0.3 mM). (A) Emission ratio images before (basal) and after treatment with 0.3 mM ML218 for 1 h. The calibration squares are as described in Figure 1. (B) Atrial (red) and ventricular (gray)  $\text{Ca}^{2+}$  levels (emission ratio) before and after treatment with ML218. The red- and gray-dashed lines indicate the start of atrial and ventricular  $\text{Ca}^{2+}$  transients, respectively. (C) AV delay before and after treatment with ML218. (D) Time course of ventricular diameter before and after treatment with ML218. In this experiment, images were acquired at 100 frames/s.

was shorter than the delay of the last conducted impulse before the block, which is a distinguishing feature of the Wenckebach phenomenon in humans. During the dropped ventricular beat, two atrial beats contributed to ventricular filling, causing a larger end-diastolic diameter (and volume) (Figure 4D). The subsequent ventricular contraction was stronger, likely because of mechano-mechanical coupling (the Frank–Starling mechanism), so that the previous end-systolic diameter was immediately reached. Note that the ventricular CaT amplitude did not increase after the dropped beat (Figure 4B). Mobitz type I AV blocks were observed at a higher frequency in 5 dpf larvae treated with 0.3 mM ML218.

Upon incubation of 3 dpf larvae with 1 mM ML218 for 1 h, atrial bradycardia and 2:1 arrhythmia were observed, with an increased amplitude of the CaT, particularly in the ventricle (Figure 3B, Table 2, Movie S13 and S14). The effect of ML218 (1 mM) on cardiac contractility and hemodynamics in 3 dpf larvae was like that observed in the 2:1 AV block induced by dofetilide: increased FAC and SV but decreased CO (Figure 3D), and ventricular filling was biphasic. However, in contrast with the  $I_{\text{Kr}}$  blockers

(Figure 1C, Table S3), in ML218 treated larvae with 2:1 arrhythmia, the AV delay increased (Figure 3C, Table 2) indicating that blocking TTCCs slows AV conduction velocity. Taken together, these results demonstrate that TTCCs are involved in the SA ring pacemaker activity and in AV conduction in the zebrafish larva heart.

Figure S2B shows that the effects of ML218 were reversible. When larvae at 3 dpf were incubated with 1 mM ML218 in E3 medium (not embedded in agarose), atrial bradycardia and 2:1 block were visible after 20 min. After 90 min washout of the drug, 70% of larvae recovered the normal 1:1 atrial to ventricular beat ratio. Atrial HR recovered slowly after washout of ML218, compared to a stable HR in untreated and DMSO-treated larvae over 24 h (Figure S2C).

### 3 | DISCUSSION

The zebrafish orthologs of hERG and TTCC that are the focus of this study may exhibit pharmacological sensitivity

that differs from mammals. The important residues for hERG blocking have been identified by Ala scanning mutagenesis. Tyr652 and Phe656 on the S6 helix, unique to ERG K<sup>+</sup> channels, are key for drug binding, whereas pore helix residues Thr623 and Ser624 are also important for binding of many compounds.<sup>38</sup> Indeed, the drug-binding region of hERG is conserved in zerg, with only one amino acid difference (Pro635 in zerg is a Ser in human/mouse ERG).<sup>14,15</sup> This explains that most drugs which prolong the QT interval in humans show 2:1 AV block when tested in zebrafish.

In the zebrafish model, the drug concentration is difficult to control and know at the cellular level. We used high drug concentrations and long incubation times compared to studies in isolated cardiomyocytes because the skin of zebrafish hampers drug diffusion. In earlier studies in embryos, QT-prolonging drugs showed time- and dose-dependent effects on HR and rhythm.<sup>15</sup> For various drugs, increasing concentration resulted in bradycardia, then 2:1 AV block and, at the highest concentration, irregular arrhythmia and higher degree AV blocks. Further, low drug concentrations often required 24-h incubation for the arrhythmias to occur, suggesting that these drugs accumulate slowly in the heart. Our results agree with these observations. Moreover, we found that the agarose embedding needed to immobilize larvae during imaging further hindered drug diffusion, since incubation of larvae without agarose shortened about five fold the time needed to see 2:1 AV block by 100 μM dofetilide (compare Figure 1 with Figure S2).

### 3.1 | ERG channels contribute to pacemaker automaticity and AV conduction

The I<sub>Kr</sub> blockers used here (dofetilide, terfenadine, astemizole, and haloperidol) are known to cause QT interval prolongation and increased risk of *torsades de pointes* in humans.<sup>14</sup> Herein, we observed that the I<sub>Kr</sub> blockers induced bradycardia, 2:1 AV block, decrease in ventricular Ca<sup>2+</sup> levels (particularly diastolic Ca<sup>2+</sup>), and, in larvae with 2:1 arrhythmia, increase in CaT amplitude, raised FAC and SV, but reduced CO due to the slow ventricular HR.

I<sub>Kr</sub> is the major outward current responsible for repolarization in adult and embryonic zebrafish cardiomyocytes,<sup>4,25</sup> as occurs in humans. Regarding the mechanism of the bradycardia observed in our results, the ERG K<sup>+</sup> channel blocker E-4031 was found to prolong the APD<sub>90</sub> in atrial and ventricular tissue of spontaneously beating hearts from adult zebrafish.<sup>25</sup> In 3 dpf zebrafish larvae expressing an optogenetic voltage biosensor in the heart, E-4031 also prolonged the APD and reduced AP frequency,<sup>39</sup>

confirming earlier reports that QT-prolonging drugs cause bradycardia in zebrafish larvae.<sup>15,40</sup> In rabbit SAN cells under current clamp, dofetilide reduced the firing rate and the slope of the pacemaker potential.<sup>31</sup> Interestingly, zerg is expressed in the sinoatrial ring in zebrafish.<sup>24</sup> Our findings on bradycardia induced by I<sub>Kr</sub> blockers agree with these reports and suggest that the zerg channel contributes to pacemaking in the sinoatrial ring in zebrafish larvae. It is possible that I<sub>Kr</sub> blockers decreased the HR by acting on other currents, like I<sub>f</sub>, in addition to blocking zerg. Nonetheless, it is unlikely that all the structurally unrelated drugs used in this study block the I<sub>f</sub> current, in addition to I<sub>Kr</sub>.

The zebrafish mutant *breakdance*, which holds a mutation in *kcnh6a*, is characterized by a 2:1 AV block.<sup>15,16</sup> In isolated paced hearts from *breakdance* larvae, voltage mapping revealed that the ventricular AP was so prolonged that every second atrial AP intruded on the refractory period of the previous ventricular beat.<sup>16</sup> A 2:1 block was also found in 3 dpf larvae incubated with various QT-prolonging drugs<sup>15</sup> and in paced wild-type embryo ventricles treated with terfenadine.<sup>33</sup> In our results, we identified the AV canal as the site of the block in dofetilide-treated larvae, since it showed CaT with a very prolonged plateau phase (Figure 1E). In addition to the conduction tissue, zebrafish ventricular cardiomyocytes also express ERG channels.<sup>4,6,25</sup> Indeed, we found that the blocked atrial beat caused little or no ventricular filling in some 3 dpf larvae and that the ventricular CaT plateau was wider: the ventricle remained contracted suggesting a prolonged APD in these cells (Figure 2B).

### 3.2 | Role of TTCCs on SA automaticity and AV conduction

In the adult mammalian heart, I<sub>Ca,T</sub> current carried by Ca<sub>v</sub>3.1 channels plays a functional role in SAN automaticity together with I<sub>f</sub> and I<sub>Ca,L</sub>, as well as in the AV node and Purkinje network.<sup>17–20,22</sup> In a recent report, inhibition of I<sub>Ca,T</sub> with Ni<sup>2+</sup> decreased the HR in isolated hearts of adult zebrafish.<sup>41</sup> In the present work, the selective TTCC blocker ML218 caused bradycardia (Figure 3B). Our results agree with the previous observations and provide evidence of the contribution of TTCCs to the SA pacemaker automaticity in zebrafish larvae.

Ca<sub>v</sub>3.1 knockout mice, which lack I<sub>Ca,T</sub> in both the SAN and AV node cells, displayed a prolonged PR interval, demonstrating the involvement of TTCCs in AV conduction.<sup>17,20</sup> Since the AV node also possesses automaticity, inactivation of Ca<sub>v</sub>3.1 channels in mice was found to slow AV node pacemaking and to produce an erratic HR.<sup>19</sup> In zebrafish larvae, transcripts encoding for TTCCs (*cacna1g*)

are enriched in the SA ring and AV canal.<sup>23,24</sup> Here, alterations in the AV conduction with dose-dependent severity were induced by blocking TTCCs in 3 dpf larvae: second-degree AV blocks of Mobitz type 1, and 2:1 AV block (Figures 3 and 4).

We propose that the AV delay measured in the Ca<sup>2+</sup> traces (the time between the start of atrial and ventricular CaT) is equivalent to the PR interval of the ECG. This delay in control larvae was 85 ± 15 ms (*n* = 57), similar to the delay measured with a potentiometric dye in isolated zebrafish hearts at 14 dpf (about 110 ms).<sup>42</sup> The AV delay was critical to distinguish between the mechanisms resulting in 2:1 arrhythmia by blocking I<sub>Kr</sub> and I<sub>Ca,T</sub>. With the I<sub>Kr</sub> blockers, the AV delay during the 2:1 arrhythmia was reduced (Figure 1C, Table 1 and Table S3), whereas the TTCC blocker increased it (Figure 3C, Table 2), in keeping with a prolonged PR interval seen in Ca<sub>v</sub>3.1 knockout mice.<sup>17,43</sup> In both cases, the CaT at the AV canal was extended during the blocked atrial beat, indicating that the atrial AP found a refractory AV canal. In conclusion, our results show that TTCCs are needed for both SA pacemaker function and AV conduction in zebrafish larvae, as has been shown in mammals.

### 3.3 | TTCCs are not essential to maintain ventricular contraction in zebrafish larvae

Contraction of myocytes in adult zebrafish has been reported to rely on sarcolemmal Ca<sup>2+</sup> influx through LTCCs and reverse mode Na/Ca exchanger.<sup>4,8,11,12</sup> We and others previously reported that the LTCC blocker nifedipine reduced Ca<sup>2+</sup> levels, CaT amplitude, and ventricular contractility in zebrafish larvae.<sup>28,39,44</sup> Although a robust I<sub>Ca,T</sub> has been described in both the atrium and ventricle of adult zebrafish, accounting for about 32% of sarcolemmal Ca<sup>2+</sup> influx,<sup>8,25</sup> its physiological significance in the working myocardium is unknown. A recent study found a physiological role of TTCCs in ventricular cardiomyocytes of adult mice.<sup>26</sup> Ni<sup>2+</sup> at a concentration which inhibits I<sub>Ca,T</sub> hardly decreased the force of contraction of zebrafish ventricular slices.<sup>45</sup> Interestingly, here we show that the TTCC blocker ML218 had no effect on CaT amplitude or contractility in larvae showing bradycardia (Figure 3). It is possible that the Ca<sup>2+</sup>-dependent inhibition of L-type Ca<sup>2+</sup> current is removed when TTCCs are blocked, which may cause a compensatory increase in Ca<sup>2+</sup> influx so that the CaT amplitude is not changed. Because of its low-voltage threshold of about -70 mV and fast inactivation, I<sub>Ca,T</sub> contributes to the early phase of the AP and CaT, in contrast with I<sub>Ca,L</sub> (-40 mV threshold).<sup>8,18</sup> Here, we found that inhibition of TTCCs increases the rise time of the CaT. It has been

suggested that early activation of TTCCs during the AP is relevant to the adaptation of the zebrafish HR to higher temperatures found in their native environment.<sup>8</sup> Thus, the function of TTCCs may be more important to ensure a fast Ca<sup>2+</sup> rise at high HR than to achieve a net Ca<sup>2+</sup> influx. Our findings suggest that Ca<sup>2+</sup> influx through TTCCs does not play a major role in the contraction of the larval zebrafish heart, despite their reported abundance in atrial and ventricular cardiomyocytes.

### 3.4 | Correlation between Ca<sup>2+</sup> and ventricular filling with the strength of contraction

The strength of cardiac contraction depends on the sympathetic tone (contractility, related to the systolic Ca<sup>2+</sup> rise) and on ventricular filling at the end of diastole (preload or end-diastolic volume). Here, drugs causing 2:1 AV block (I<sub>Kr</sub> blockers and the TTCC blocker ML218), by decreasing ventricular HR to half, decreased diastolic Ca<sup>2+</sup> levels, raised CaT amplitude, and increased the SV due to an increased preload (Figures 1D and 3D, Figures S1D and S3C, Tables 1 and 2 and Table S3). In contrast to mammals, the teleost atrium plays a crucial role in ventricular filling, which depends on atrial contraction rather than on venous pressure.<sup>46</sup> In 2:1 arrhythmia caused by ML218, two atrial beats fed the ventricle before its contraction so that the FAC and SV increased (Figure 3D). This result is consistent with mechano-mechanical coupling (Frank-Starling mechanism): stretching of the ventricle caused a stronger contraction; this effect was particularly clear in Figure 4D. It was recently shown that acute atrial dilation in 2 dpf zebrafish by injection of a given volume into the venous circulation upstream of the heart increased the atrial stroke area, suggesting that mechano-mechanical coupling drives the adaptive increase in atrial output during development.<sup>30</sup> These and the present results highlight the advantage of the zebrafish model to investigate cardiac performance in vivo.

### 3.5 | Zebrafish larvae as a model to study the function of repolarization and Ca<sup>2+</sup> currents

Zebrafish embryos and larvae have been proposed as an in vivo model to study cardiac physiology, pathophysiology, and drug discovery.<sup>1-3,6,7,47</sup> However, whether findings in this vertebrate animal model can be extrapolated to understand human disease mechanisms must be carefully considered since there are differences among isoforms of several ion channel types.<sup>5,8</sup> A zebrafish-based screening platform

has been proposed for early assessment of cardiovascular toxicity during drug discovery.<sup>48,49</sup> Besides, in a comparative quantitative analysis of the *in vivo* cardiovascular responses of zebrafish, rat, dog, and human to the model drugs propranolol, losartan, and captopril, zebrafish and human responses were comparable in >80% of drug combinations.<sup>50</sup> These reports suggest the translatability of cardiovascular drug responses in the zebrafish model to the human. Since TTCCs are abundantly expressed in zebrafish, our results suggest that this model will allow examination of the role of  $I_{Ca,T}$  as a potential drug target in human fetal or neonatal heart disease, and in hypertrophy and heart failure in adults, when these channels are re-expressed.<sup>8</sup>

## 4 | MATERIALS AND METHODS

### 4.1 | Ethical approval

All procedures were approved by the Consejería de Agricultura, Agua y Desarrollo Rural, Junta de Comunidades de Castilla-La Mancha, Spain (document dated March 16, 2020). Zebrafish husbandry was carried out following standard procedures in compliance with national and EU regulations (RD 53/2013, Spain).

### 4.2 | Zebrafish husbandry

Zebrafish were kept in the Center for Animal Experimentation of the Albacete School of Medicine with a light/dark cycle of 14/10h. Fertilized zebrafish eggs in synchronized stage were obtained following standard procedures. Zebrafish eggs and larvae were maintained in E3 medium (5 mM NaCl, 0.17 mM KCl, 0.33 mM  $MgSO_4$ , 0.33 mM  $CaCl_2$ , pH 7.4 in double-distilled  $H_2O$ ) at 28.5°C. No methylene blue was added to E3 medium to decrease larva autofluorescence.

### 4.3 | Zebrafish transgenic lines

The following fish lines expressing ratiometric  $Ca^{2+}$  biosensors were used: *Tg(myl7:Twitch-4)*,<sup>28</sup> *Tg(myl7:mCyRFP1-GCaMP6f)*,<sup>29</sup> and *Tg(myl7:Twitch-1)* (this study).

### 4.4 | Generation of the transgenic line *Tg(myl7:Twitch-1)*

The ratiometric  $Ca^{2+}$  biosensor Twitch-1<sup>37</sup> was cloned into the pT2A-Tol2-myl7 transposon vector as previously

described.<sup>44</sup> To generate stable transgenic zebrafish, single-cell wild-type AB embryos were injected with a mixture of pTol2-myl7:Twitch-1 and transposase mRNA each at a concentration of 12.5 ng/ $\mu$ L. For transposase mRNA production, the pCS-zT2TP construct<sup>51</sup> was linearized via ApaI digestion, and *in vitro* transcription was carried out using the mMESSAGING mMACHINE SP6 kit (Ambion Inc.). Injected embryos (F0) were screened by fluorescence in the heart and grown to adulthood. Adult F0 fish were outcrossed to wild-type AB zebrafish to identify founders with insertions in the germline by the presence of cardiac fluorescence in their offspring (F1). Fluorescent F1 fish were outcrossed to wild-type AB zebrafish, and F2 larvae expressing Twitch-1 were raised to adulthood. Adult F2 fish were crossed again with adult wild-type AB zebrafish to obtain F3 *Tg(myl7:Twitch-1)* embryos, which were used for imaging.

### 4.5 | Mounting of larvae for microscopy

Non-anesthetized 3, 4, and 5 dpf larvae were embedded in 100  $\mu$ L of 0.3% low melting point agarose in E3 medium and gelled on 96-square well plates and flat clear bottom (ibidi) (one larva per well). Larvae at 3 and 4 dpf were mounted ventral-side down and, at 5 dpf, right-side down to visualize atrium and ventricle in the same plane. Once the agarose solidified, 100  $\mu$ L of E3 medium was added to each well and larvae were incubated for 30 min at 28°C to get a stable HR. Where indicated, larvae were incubated with 75  $\mu$ M of the myosin inhibitor *para*-aminoblebbistatin (Optopharma) for 2 h before mounting for microscopy.

### 4.6 | Ratiometric fluorescence imaging

We acquired fluorescence images of the beating heart of 3, 4, and 5 dpf larvae with a wide-field microscope (DMIRE-2, Leica Microsystems) equipped with a sCMOS camera (ORCA-Flash 4.0), controlled by Aquacosmos 2.6 (both from Hamamatsu Photonics) as previously described.<sup>28,29</sup> The image acquisition rate was 50 frames/s (20 ms integration per image) during 5–10 s; some larvae were imaged at 100 frames/s. Larvae under the microscope stage were kept at 28°C in a chamber incubator (PeCon GmbH). Excitation source and optical elements for Twitch-4 and Twitch-1 were as described in Salgado-Almario et al.<sup>28</sup> and for mCyRFP1-GCaMP6f as in Vicente et al.<sup>29</sup> The short- and long-wavelength emission images of these biosensors were acquired simultaneously with an image splitter (W-View Gemini, Hamamatsu Photonics).

## 4.7 | Drug treatment

Dofetilide (Tocris 3757), terfenadine (Tocris 3948), astemizole (Tocris 3489), haloperidol hydrochloride (Tocris 0931), and ML218 hydrochloride (Tocris 4507) stock solutions were made in dimethyl sulfoxide (DMSO) and diluted in E3 medium at 28°C. After recording basal images, 100 µL of drugs diluted in E3 medium were added to the well, and new sets of images were recorded. High drug concentrations were used since the skin and the agarose layer, where larvae are embedded, slow down diffusion and access of the drug to the heart.<sup>15,28,39</sup> For treatment with terfenadine, embryos at 1 dpf were placed in 0.003% N-phenylthiourea (Sigma-Aldrich P7690) in E3 medium to prevent pigmentation. At 3 dpf, larvae were transferred to a N-phenylthiourea solution containing 20 µM terfenadine or 0.04% DMSO and incubated for 24 h.

## 4.8 | Ratio image processing and data analysis

Ratiometric images and ratio data were processed and analyzed with the custom software Ratioscope 8.31 (doi.org/10.25493/5G5V-HBC) written in the IGOR Pro environment (WaveMetrics, OR, USA) as reported in Salgado-Almario et al.<sup>28</sup> In short, ratio images were calculated pixel-by-pixel at each time point (YFP/CFP emission ratio for the FRET indicators; *GCaMP6f/mCyrFP1* emission ratio for *mCyrFP1-GCaMP6f*). Regions of interest (ROI) were drawn over the atrium and the ventricle, and the ratio value of each was calculated by averaging all the pixels' values weighted by the average intensity of the two emission channels in each pixel.<sup>52,53</sup> Thus, background, dim pixels contributed little to the computed ratio and thresholding was not needed for display.

## 4.9 | Automatic calculation of kinetic parameters of the Ca<sup>2+</sup> transients

Several kinetic parameters were automatically calculated from the ratio traces with the software Ratioscope 8.31 in IGOR Pro: diastolic ratio, systolic ratio, ratio amplitude (systolic minus diastolic ratio), and HR of the CaT (in bpm). Data shown for each larva represent the average of all the cardiac cycles in 5 or 10s of continuous recording. We calculated the AV delay of the Ca<sup>2+</sup> transients by subtracting the start time of the atrial CaT from that of the ventricular CaT. This parameter is analogous to the

PR interval of the ECG (the delay between atrial and ventricular electrical excitation).

## 4.10 | Automatic measurement of ventricular diameter

To monitor the ventricular filling and contraction, we wrote an analysis program in IGOR Pro that automatically measures changes in the ventricular diameter throughout the cardiac cycle. A line drawn through the ventricle in the fluorescence images tracks the movement of the wall, and the displacement of the ventricular walls is represented in a kymogram. The external wall was used to measure the ventricular diameter since the inner wall did not provide sufficient contrast owing to trabeculation.

## 4.11 | Measurement of contractile and hemodynamic parameters

To calculate contractile parameters, we measured the ventricular end-systolic and end-diastolic areas and major diameters in systole and diastole by drawing ROIs. These area measurements were used to calculate the fractional area change (FAC).

$$\text{FAC} = \frac{(\text{end diastolic area} - \text{end systolic area})}{\text{end diastolic area}}$$

To analyze the hemodynamic parameters, we estimated the ventricular end-systolic and end-diastolic volumes with the formula of an ellipsoid of revolution, assuming that the diameter in the z-axis matched the minor diameter in the imaging plane:

$$\text{Volume} = 4/3 \times \text{minor radius} \times \text{ventricular area}$$

The minor end-systolic and end-diastolic diameters were calculated assuming that the ventricle in the focal plane is an ellipse of equal area and major diameter as those measured with ROIs:

$$\text{Area of ellipse} = \pi \times \text{minor radius} \times \text{major radius}$$

$$\text{Minor radius} = \frac{\text{Area of an ellipse}}{(\pi \times \text{major radius})}$$

The hemodynamic parameters were

$$\text{Stroke volume (SV)} = \text{end diastolic volume} - \text{end systolic volume}$$

$$\text{Cardiac output (CO)} = \text{SV} \times \text{HR}$$

## 4.12 | Statistics

Statistical analysis was done with GraphPad Prism 8 (GraphPad Software) and Igor Pro (WaveMetrics). The Shapiro–Wilk test was used to test for normality. In case of normal distribution, the differences between two groups were analyzed using the paired Student's *t* test. Comparisons between multiple experimental groups were analyzed by one-way ANOVA with Dunnett's multiple comparisons post-test for paired data or with Tukey's multiple comparisons post-test for unpaired data. In case of non-normal distribution, the differences between two groups of paired data were analyzed using the Wilcoxon test. Comparisons between multiple experimental groups were analyzed by the Friedman test with Dunn's multiple comparisons post-test for paired data, or by the Kruskal–Wallis test with Dunn's multiple comparisons post-test for unpaired data. The number of independent experiments (experimental days, *N*) and the number of larvae (*n*) are indicated in the figure legends. Data are shown as the mean ± SD. A *p* < 0.05 was considered statistically significant (\**p* < 0.05, †*p* < 0.01, ‡*p* < 0.001).

## 4.13 | Conclusion

The present results show the potential of the transgenic lines expressing ratiometric Ca<sup>2+</sup> biosensors in the heart to investigate the function of ion channels and their mechanical impact in the zebrafish model. Our results suggest that the I<sub>Kr</sub> current plays similar roles in zebrafish and mammals and that I<sub>Kr</sub> blockers primarily hinder conduction along the AV canal but can also extend the refractory period of working ventricular myocytes. Moreover, as it happens in mammals, TTCCs are involved in the SA pacemaker and in AV conduction in zebrafish larvae. In contrast with LTCCs, inhibition of TTCCs seems not to decrease the force of ventricular contraction. Since zebrafish larvae allow high-throughput drug screening,<sup>40,48,54</sup> the lines expressing Ca<sup>2+</sup> biosensors in the heart could also be used to identify anti-arrhythmic compounds. Furthermore, the ease of gene modification in zebrafish may allow the study of the mechanism of genetic arrhythmias in personalized medicine.

## AUTHOR CONTRIBUTIONS

**Jussep Salgado-Almarío:** Conceptualization; methodology; validation; formal analysis; investigation; data curation; writing – original draft; writing – review and editing; visualization. **Yillcer Molina:** Investigation. **Manuel Vicente:** Methodology; investigation; writing – review and editing. **Antonio Martínez-Sielva:** Methodology; investigation. **Raúl Rodríguez-García:** Investigation.

**Pierre Vincent:** Software; writing – review and editing. **Beatriz Domingo:** Methodology; validation; resources; data curation; writing – review and editing; supervision; funding acquisition; project administration; conceptualization. **Juan Llopis:** Conceptualization; methodology; validation; resources; supervision; data curation; writing – review and editing; project administration; funding acquisition; writing – original draft.

## ACKNOWLEDGMENTS

We thank Carmen Cifuentes for expert technical assistance and Angela Nieto, Ana Gomez, and Paola Mercedes Brown for critical review of the manuscript.

## CONFLICT OF INTEREST STATEMENT

The authors declare no conflict of interest.

## FUNDING INFORMATION

This work was supported by the Ministry of Science, Innovation and Universities, Spain [PID2019-111456RB-100 to J.L.]; the Consejería de Educación, Cultura y Deportes, Junta de Comunidades de Castilla-La Mancha, co-funded by EU FEDER-ERDF [SBPLY/19/180501/000223 to J.L. and B.D.]; and the University of Castilla-La Mancha, co-funded by EU FEDER-ERDF [2019-GRIN-27019, 2020-GRIN-29186, and 2021-GRIN-31151 to J.L.].

## DATA AVAILABILITY STATEMENT

The data that support the findings of this study are available from the corresponding author upon reasonable request.

## ORCID


Jussep Salgado-Almarío  <https://orcid.org/0000-0002-7421-6168>

Yillcer Molina  <https://orcid.org/0000-0003-3425-4503>

Manuel Vicente  <https://orcid.org/0000-0002-9464-918X>

Antonio Martínez-Sielva  <https://orcid.org/0000-0002-1337-308X>

Pierre Vincent  <https://orcid.org/0000-0002-8479-1908>

Beatriz Domingo  <https://orcid.org/0000-0001-9430-4803>

Juan Llopis  <https://orcid.org/0000-0002-9460-0642>

## REFERENCES

1. Parker T, Libourel PA, Hetheridge MJ, et al. A multi-endpoint in vivo larval zebrafish (*Danio rerio*) model for the assessment of integrated cardiovascular function. *J Pharmacol Toxicol Methods*. 2014;69(1):30-38.
2. Bowley G, Kugler E, Wilkinson R, et al. Zebrafish as a tractable model of human cardiovascular disease. *Br J Pharmacol*. 2022;179(5):900-917.

3. Genge CE, Lin E, Lee L, et al. The zebrafish heart as a model of mammalian cardiac function. *Rev Physiol Biochem Pharmacol*. 2016;171:99-136.
4. Alday A, Alonso H, Gallego M, et al. Ionic channels underlying the ventricular action potential in zebrafish embryo. *Pharmacol Res*. 2014;84:26-31.
5. van Opbergen CJM, van der Voorn SM, Vos MA, de Boer TP, van Veen TAB. Cardiac Ca(2+) signalling in zebrafish: translation of findings to man. *Prog Biophys Mol Biol*. 2018;138:45-58.
6. Vornanen M, Hassinen M. Zebrafish heart as a model for human cardiac electrophysiology. *Channels (Austin)*. 2016;10(2):101-110.
7. Ravens U. Ionic basis of cardiac electrophysiology in zebrafish compared to human hearts. *Prog Biophys Mol Biol*. 2018;138:38-44.
8. Haverinen J, Hassinen M, Dash SN, Vornanen M. Expression of calcium channel transcripts in the zebrafish heart: dominance of T-type channels. *J Exp Biol*. 2018;221(Pt 10):jeb179226.
9. Milan DJ, Jones IL, Ellinor PT, MacRae CA. In vivo recording of adult zebrafish electrocardiogram and assessment of drug-induced QT prolongation. *Am J Physiol Heart Circ Physiol*. 2006;291(1):H269-H273.
10. Liu CC, Li L, Lam YW, Siu CW, Cheng SH. Improvement of surface ECG recording in adult zebrafish reveals that the value of this model exceeds our expectation. *Sci Rep*. 2016;6:25073.
11. Bovo E, Dvornikov AV, Mazurek SR, de Tombe PP, Zima AV. Mechanisms of Ca(2+) handling in zebrafish ventricular myocytes. *Pflugers Arch*. 2013;465(12):1775-1784.
12. Zhang PC, Llach A, Sheng XY, Hove-Madsen L, Tibbits GF. Calcium handling in zebrafish ventricular myocytes. *Am J Physiol Regul Integr Comp Physiol*. 2011;300(1):R56-R66.
13. Leong IU, Skinner JR, Shelling AN, Love DR. Identification and expression analysis of *kcnh2* genes in the zebrafish. *Biochem Biophys Res Commun*. 2010;396(4):817-824.
14. Kannankeril P, Roden DM, Darbar D. Drug-induced long QT syndrome. *Pharmacol Rev*. 2010;62(4):760-781.
15. Langheinrich U, Vacun G, Wagner T. Zebrafish embryos express an orthologue of HERG and are sensitive toward a range of QT-prolonging drugs inducing severe arrhythmia. *Toxicol Appl Pharmacol*. 2003;193(3):370-382.
16. Milan DJ, Kim AM, Winterfield JR, et al. Drug-sensitized zebrafish screen identifies multiple genes, including *GINS3*, as regulators of myocardial repolarization. *Circulation*. 2009;120(7):553-559.
17. Mangoni ME, Traboulsie A, Leoni AL, et al. Bradycardia and slowing of the atrioventricular conduction in mice lacking Cav3.1/alpha1G T-type calcium channels. *Circ Res*. 2006;98(11):1422-1430.
18. Ono K, Iijima T. Cardiac T-type Ca(2+) channels in the heart. *J Mol Cell Cardiol*. 2010;48(1):65-70.
19. Marger L, Mesirca P, Alig J, et al. Functional roles of Ca(v)1.3, Ca(v)3.1 and HCN channels in automaticity of mouse atrioventricular cells: insights into the atrioventricular pacemaker mechanism. *Channels*. 2011;5(3):251-261.
20. Baudot M, Torre E, Bidaud I, et al. Concomitant genetic ablation of L-type Cav1.3 (alpha1D) and T-type Cav3.1 (alpha1G) Ca(2+) channels disrupts heart automaticity. *Sci Rep*. 2020;10(1):18906.
21. Boutjdir M. Molecular and ionic basis of congenital complete heart block. *Trends Cardiovasc Med*. 2000;10(3):114-122.
22. Mesirca P, Torrente AG, Mangoni ME. Functional role of voltage gated Ca(2+) channels in heart automaticity. *Front Physiol*. 2015;6:19.
23. Abu Nahia K, Migdal M, Quinn TA, et al. Genomic and physiological analyses of the zebrafish atrioventricular canal reveal molecular building blocks of the secondary pacemaker region. *Cell Mol Life Sci*. 2021;78(19-20):6669-6687.
24. Minhas R, Loeffler-Wirth H, Siddiqui YH, et al. Transcriptome profile of the sinoatrial ring reveals conserved and novel genetic programs of the zebrafish pacemaker. *BMC Genomics*. 2021;22(1):715.
25. Nemtsas P, Wettwer E, Christ T, Weidinger G, Ravens U. Adult zebrafish heart as a model for human heart? An electrophysiological study. *J Mol Cell Cardiol*. 2010;48(1):161-171.
26. Marksteiner J, Ebner J, Salzer I, et al. Evidence for a physiological role of T-type Ca channels in ventricular cardiomyocytes of adult mice. *Membranes (Basel)*. 2022;12(6):566.
27. Eisner DA, Caldwell JL, Kistamás K, Trafford AW. Calcium and excitation-contraction coupling in the heart. *Circ Res*. 2017;121(2):181-195.
28. Salgado-Almario J, Vicente M, Molina Y, et al. Simultaneous imaging of calcium and contraction in the beating heart of zebrafish larvae. *Theranostics*. 2022;12(3):1012-1029.
29. Vicente M, Salgado-Almario J, Valiente-Gabioud AA, et al. Early calcium and cardiac contraction defects in a model of phospholamban R9C mutation in zebrafish. *J Mol Cell Cardiol*. 2022;173:127-140.
30. Baillie JS, Gendernalik A, Garrity DM, Bark D Jr, Quinn TA. The in vivo study of cardiac mechano-electric and mechano-mechanical coupling during heart development in zebrafish. *Front Physiol*. 2023;14:1086050.
31. Tohse N, Kanno M. Effects of dofetilide on membrane currents in sinoatrial node cells of rabbit. *Jpn J Pharmacol*. 1995;69(4):303-309.
32. Lu HR, Hermans AN, Gallacher DJ. Does terfenadine-induced ventricular tachycardia/fibrillation directly relate to its QT prolongation and Torsades de Pointes? *Br J Pharmacol*. 2012;166(4):1490-1502.
33. Arnaout R, Ferrer T, Huisken J, et al. Zebrafish model for human long QT syndrome. *Proc Natl Acad Sci USA*. 2007;104(27):11316-11321.
34. Gu G, Na Y, Chung H, Seok SH, Lee HY. Zebrafish larvae model of dilated cardiomyopathy induced by terfenadine. *Korean Circ J*. 2017;47(6):960-969.
35. Quan H, Oh GC, Seok SH, Lee HY. Fimasartan, an angiotensin II receptor antagonist, ameliorates an in vivo zebrafish model of heart failure. *Korean J Intern Med*. 2020;35(6):1400-1410.
36. Vicente M, Salgado-Almario J, Collins MM, et al. Cardioluminescence in transgenic zebrafish larvae: a calcium imaging tool to study drug effects and pathological modeling. *Biomedicine*. 2021;9(10):1294.
37. Thestrup T, Litzlbauer J, Bartholomäus I, et al. Optimized ratiometric calcium sensors for functional in vivo imaging of neurons and T lymphocytes. *Nat Methods*. 2014;11(2):175-182.
38. Mitcheson JS. hERG potassium channels and the structural basis of drug-induced arrhythmias. *Chem Res Toxicol*. 2008;21(5):1005-1010.
39. van Opbergen CJM, Koopman CD, Kok BJM, et al. Optogenetic sensors in the zebrafish heart: a novel in vivo electrophysiological tool to study cardiac arrhythmogenesis. *Theranostics*. 2018;8(17):4750-4764.
40. Milan DJ, Peterson TA, Ruskin JN, Peterson RT, MacRae CA. Drugs that induce repolarization abnormalities cause bradycardia in zebrafish. *Circulation*. 2003;107(10):1355-1358.



41. Stoyek MR, MacDonald EA, Mantifel M, et al. Drivers of sinoatrial node automaticity in zebrafish: comparison with mechanisms of mammalian pacemaker function. *Front Physiol.* 2022;13:818122.
42. Sacconi L, Silvestri L, Rodriguez EC, et al. KHz-rate volumetric voltage imaging of the whole Zebrafish heart. *Biophys Rep (N Y).* 2022;2(1):100046.
43. Mesirca P, Torrente AG, Mangoni ME. T-type channels in the sino-atrial and atrioventricular pacemaker mechanism. *Pflugers Arch.* 2014;466(4):791-799.
44. Salgado-Almario J, Vicente M, Vincent P, Domingo B, Llopis J. Mapping calcium dynamics in the heart of zebrafish embryos with ratiometric genetically encoded calcium indicators. *Int J Mol Sci.* 2020;21(18):6610.
45. Haustein M, Hannes T, Trieschmann J, et al. Excitation-contraction coupling in zebrafish ventricular myocardium is regulated by trans-sarcolemmal  $\text{Ca}^{2+}$  influx and sarcoplasmic reticulum  $\text{Ca}^{2+}$  release. *PLoS One.* 2015;10(5):e0125654.
46. Lee L, Genge CE, Cua M, et al. Functional assessment of cardiac responses of adult zebrafish (*Danio rerio*) to acute and chronic temperature change using high-resolution echocardiography. *PLoS One.* 2016;11(1):e0145163.
47. Gauvrit S, Bossaer J, Lee J, Collins MM. Modeling human cardiac arrhythmias: insights from zebrafish. *J Cardiovasc Dev Dis.* 2022;9(1):13.
48. Dyballa S, Minana R, Rubio-Brotons M, et al. Comparison of zebrafish larvae and hiPSC cardiomyocytes for predicting drug induced cardiotoxicity in humans. *Toxicol Sci.* 2019;171:283-295.
49. Maciag M, Wnorowski A, Mierzejewska M, Plazinska A. Pharmacological assessment of zebrafish-based cardiotoxicity models. *Biomed Pharmacother.* 2022;148:112695.
50. Margiotta-Casaluci L, Owen SF, Rand-Weaver M, Winter MJ. Testing the translational power of the zebrafish: an interspecies analysis of responses to cardiovascular drugs. *Front Pharmacol.* 2019;10:893.
51. Urasaki A, Morvan G, Kawakami K. Functional dissection of the Tol2 transposable element identified the minimal cis-sequence and a highly repetitive sequence in the subterminal region essential for transposition. *Genetics.* 2006;174(2):639-649.
52. Tsien RY, Harootyanian AT. Practical design criteria for a dynamic ratio imaging system. *Cell Calcium.* 1990;11(2-3):93-109.
53. Polito M, Vincent P, Guiot E. Biosensor imaging in brain slice preparations. *Methods Mol Biol.* 2014;1071:175-194.
54. Burns CG, Milan DJ, Grande EJ, Rottbauer W, MacRae CA, Fishman MC. High-throughput assay for small molecules that modulate zebrafish embryonic heart rate. *Nat Chem Biol.* 2005;1(5):263-264.

## SUPPORTING INFORMATION

Additional supporting information can be found online in the Supporting Information section at the end of this article.

**How to cite this article:** Salgado-Almario J, Molina Y, Vicente M, et al. ERG potassium channels and T-type calcium channels contribute to the pacemaker and atrioventricular conduction in zebrafish larvae. *Acta Physiol.* 2024;240:e14075. doi:[10.1111/apha.14075](https://doi.org/10.1111/apha.14075)